Applied Mathematical Sciences, Vol. 7, 2013, no. 104, 5151 - 5164
HIKARI Ltd, www.m-hikari.com
http://dx.doi.org/10.12988/ams.2013.37392

A Numerical Study on Microwave Coagulation Therapy

Amy J. Liu[†], Hong Zhou[*] and Wei Kang[*]

Department of Applied Mathematics
Naval Postgraduate School
Monterey, CA 93943, USA

Abstract

Microwave coagulation therapy is a clinical technique for treating hepatocellular carcinoma (small size liver tumor). Through extensive numerical simulations, we reveal the mathematical relationships between some critical parameters in the therapy, including input power, frequency, temperature, and regions of impact. It is shown that these relationships can be approximated using simple polynomial functions. Compared to solutions of partial differential equations, these functions are significantly easier to compute and simpler to analyze for engineering design and clinical applications.

Keywords: Microwave coagulation therapy, simulation, numerical approximation

---

[†] High school student intern, currently a senior at Oakwood High School, Morgan Hill, California
[*] Professor
Disclaimer: The views expressed in this document are those of the authors and do not reflect the official policy or position of the Department of Defense or the U.S. Government.

1. Introduction

In hyperthermic oncology, tumors are treated by applying localized heat to cancerous tissues, often in combination with chemotherapy or radiotherapy. Microwave coagulation therapy is one such clinical technique for treating hepatocellular carcinoma. In the treatment, a thin microwave antenna is inserted into the cancerous tissue and the microwave energy heats up the tumor, killing the cancer cells by producing a coagulated region. Numerical models of microwave cancer therapy have been studied for many years with mature algorithms and software packages [1-6]. Despite this, the relationships between numerous parameters such as input power, frequency, temperature, and regions of impact are modeled with partial differential equations, which are not ideal or convenient for engineering design and clinical applications. However, the relationships between some of the critical parameters are relatively simple. They can be numerically represented by polynomial functions. The goal of this study is to investigate some relationships between aforementioned parameters for microwave coagulation therapy.

This study is carried out based on a large number of numerical experiments using the commercial software COMSOL [7]. The Microwave Cancer Therapy model, involving the RF and Heat Transfer modules, is used to obtain the temperature distribution in the cancerous tissues. Based on the numerical results, several functions from the model are approximated, including input power vs. maximum temperature, frequency vs. maximum temperature, and input power vs. regions of impact. These functions are either smooth and simple, or can be approximated using polynomials of degree less than or equal to nine. This set of functions provides a reduced model of microwave cancer therapy for engineering and clinical applications.

In Section 2, the basic design of a coaxial slot antenna and its numerical model are briefly described. In Section 3, the computational algorithm is tested using two different grids. We then show some numerical results for maximum temperature as a function of input power and of electromagnetic wave frequency. Their relationships are examined. In Section 4, regions of impact, including impact radius, area, and volume, for a given tissue temperature as functions of input power are presented. Conclusions are given in Section 5.

2. Microwave coagulation therapy using coaxial slot antenna

Microwave coagulation therapy is a widely used technology for the treatment of hepatocellular carcinoma. The technique has the advantage of being minimally invasive, requiring relatively short recovery time. In the treatment, a thin microwave

antenna is inserted into the tumor. Then the microwave energy provided by the antenna heats up the tumor to about 50°C to destroy cancer cells. Medical applications of microwaves and their numerical models have been actively studied and developed for many years, see [1-6] and the references therein. The antenna consists of a thin coaxial cable in a catheter. As shown in Figure 1, the cable has two layers of conductors. There is a ring-shaped slot cut in the outer conductor near the tip. All physical dimensions of the antenna are also given in Figure 1.

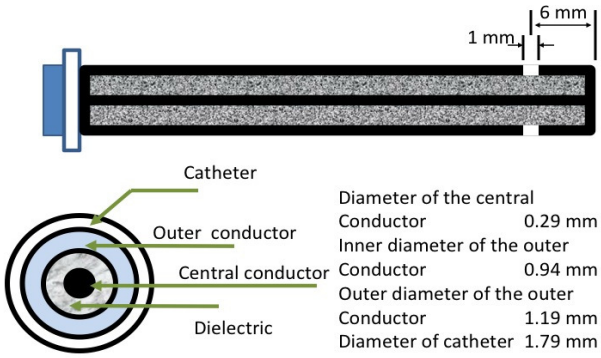

Figure 1: The structure of a coaxial ring-slot antenna and its cross section

In this study, we adopt the commercial software COMSOL [5] as a numerical model. We first solve the Maxwell equations and compute the electromagnetic specific absorption rate. Results are then used to solve the bioheat equation to obtain the temperature distribution in the cancerous tissues.

Let $\vec{E}$ and $\vec{H}$ denote the electric and magnetic field vectors, and r, φ, z the cylindrical coordinates centered on the axis of the coaxial cable. The subscript 0 of a quantity represents the value of that quantity in the free space, and the subscript r represents the relative value (ratio) of that quantity to the free space value. We model the antenna using an axisymmetric transverse magnetic (TM) formulation. For a cylindrical harmonic wave propagating in a coaxial cable, the electric and magnetic fields can be expressed as

$$\vec{E} = \frac{A}{r} e^{j(\omega t - kz)} \vec{e}_r \quad \text{and} \quad \vec{H} = \frac{A}{rZ} e^{j(\omega t - kz)} \vec{e}_\phi, \tag{1}$$

where A, ω, and k are the amplitude, angular frequency, and wave number, respectively. The impedance of the wave in the dielectric of the cable $Z = \sqrt{\frac{\mu}{\varepsilon}}$ is

equal to the square root of the ratio of the dielectric permeability μ and permittivity ε. The time-averaged power flow in the cable along the z direction between the inner radius r_{inner} and outer radius r_{outer} of the dielectric is given by

$$\vec{P}_{avg} = \int_{r_{inner}}^{r_{outer}} \mathrm{Re}[\frac{1}{2}\vec{E}\times\vec{H}^{*}]2\pi r dr = \pi\frac{A^2}{Z}\ln\frac{r_{outer}}{r_{inner}}\vec{e}_z . \tag{2}$$

In the TM formulation, the Maxwell equations can be simplified to a wave equation in H_φ

$$\nabla\times\left[\left(\varepsilon_r - \frac{j\sigma}{\omega\varepsilon_0}\right)^{-1}\nabla\times\vec{H}_\phi\right] - \mu_r {k_0}^2\vec{H}_\phi = 0 , \tag{3}$$

where σ is the electric conductivity. The electric field $\vec{E}$ is obtained from the Maxwell equations (Ampère's law) once the magnetic field $\vec{H}$ is solved from Eq. (3). Let $\vec{n}$ denote the unit normal vector for a surface. The boundary condition for a metallic surface is

$$\vec{n}\times\vec{E} = 0 . \tag{4}$$

In COMSOL, a first-order low-reflecting boundary condition

$$\vec{n}\times\sqrt{\varepsilon}\vec{E} - \sqrt{\mu}\vec{H}_\phi = -2\sqrt{\mu}\vec{H}_{\phi 0} \tag{5}$$

is used at outer boundaries of tissue. The quantity $\vec{H}_{\phi 0}$ is related to the input power $\vec{P}_{avg}$ through Eqs. (1) and (2).

The temperature distribution inside a biological tissue during the coagulation can be obtained by solving the bioheat equation [8]

$$\rho c\frac{\partial T}{\partial t} = \nabla\cdot(\kappa\nabla T) + Q_{ext} - Q_{pfu} + Q_{met} , \tag{6}$$

where ρ is the mass density, c is the specific heat capacity, T is the temperature, and κ is the thermal conductivity of the tissue, respectively. The first term on the right-hand side of Eq. (6) denotes the thermal conduction of tissue. The second term Q_{ext} is the absorbed energy due to resistive heat generated by the electromagnetic

field in tissue, which is obtained from the solution of the Maxwell equation

$$Q_{ext} = \frac{1}{2}\mathrm{Re}[(\sigma - j\omega\varepsilon)\vec{E}\cdot\vec{E}^{*}]. \tag{7}$$

When normalized by tissue density, $\frac{Q_{ext}}{\rho}$ is referred as the specific absorption rate (SAR). The third term Q_{pfu} is the heat loss due to microvascular blood perfusion,

$$Q_{pfu} = \rho_b c_b \omega_b (T - T_b), \tag{8}$$

where ρ_b is the blood density, c_b is the blood specific heat capacity, ω_b is the blood perfusion rate, and T_b is the blood temperature. The metabolic heat generation term Q_{met} is neglected in this study since its magnitude is substantially smaller than other terms in Eq. (6). In COMSOL, the time varying term on the left-hand side of Eq. (6) is also neglected, and only steady-state solutions are available. We, therefore, carry out only the stationary heat transfer problem in the current study. At boundaries, we assume no heat flux across tissue surfaces, that is

$$\vec{n}\cdot\nabla T = 0. \tag{9}$$

Dielectric, thermal, and blood perfusion properties of normal and cancerous tissues are complex functions of electromagnetic wave frequency, water and protein contents of the tissue, and temperature. These properties are obtained mostly through experimental measurements. However, measurements at temperatures above 60°C are scarce. In the current version of software, COSMOL has not implemented any of these property functions. We therefore use fixed, steady-state values in our study. Table 1 lists the properties of a liver tumor used in this study.

Table 1. Dielectric, thermal, and blood perfusion parameters for a cancerous liver tissue

dielectric permittivity	$\varepsilon = 43.03\ F/m$	blood density	$\rho = 10^3\ kg/m^3$
dielectric conductivity	$\sigma = 1.69\ S/m$	blood specific capacity	$c_b = 3639\ J/(kg\ K)$
thermal conductivity	$k = 0.56\ W/(m\,K)$	blood perfusion rate	$\omega_b = 0.0036/s$

3. Numerical experiments on the maximum temperature

In COMSOL, Eqs. (3) and (6) are solved using a finite-element method. Solutions of these differential equations have complex features around the antenna and inside the slot. Before extensive numerical experiments are carried out, we must confirm that the numerical results have converged as the grids are refined. For this purpose, we tested several grid resolutions. Two sets of grid meshes, the default grid and a refined grid, are shown in Figure 2. The former has one grid cell in the slot in the radial direction, while the latter has 10 cells. A close-up view of each grid near the slot is depicted in Figure 3.

(a) Default grid (b) Refined grid

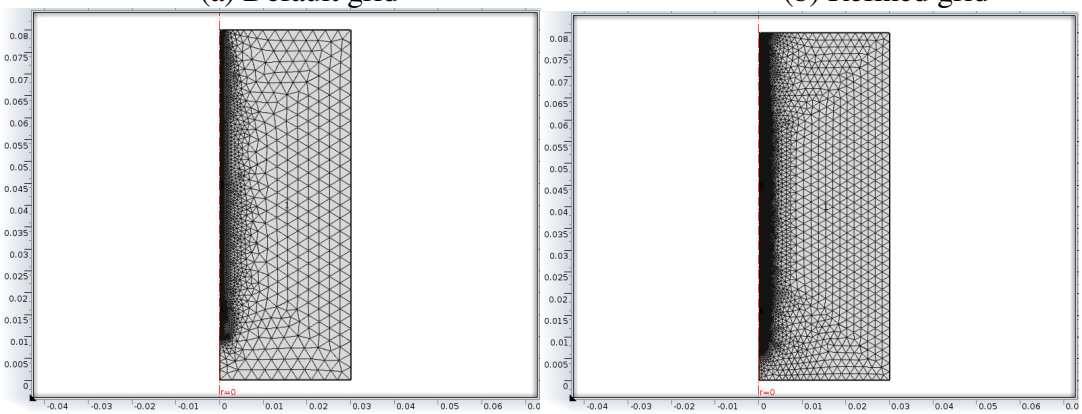

Figure 2. Two sets of grid meshes

(a) Default grid (b) Refined grid

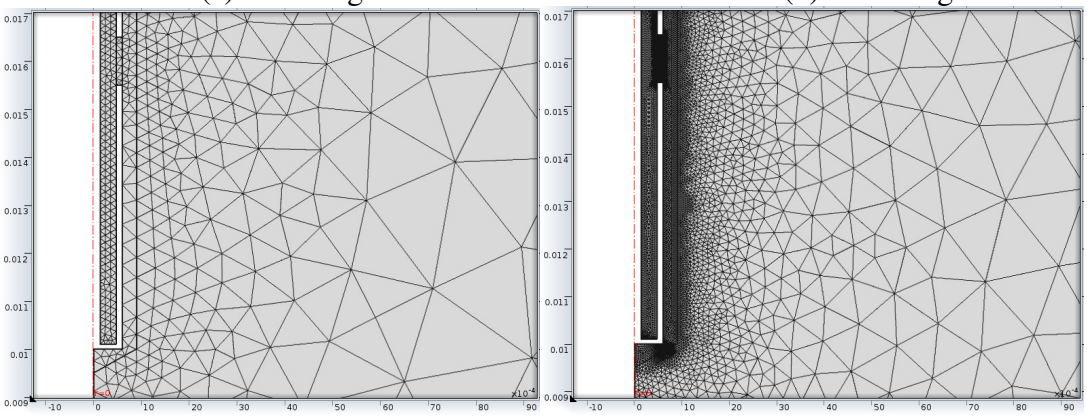

Figure 3. Close-up view of grid meshes near slot

We analyzed the electromagnetic fields, power dissipation density, and tissue temperature distributions using a cylindrical harmonic microwave. Both grids result in almost identical solutions. Some results are shown in Figures 4-7. All trials were done with input power $P = 10$ W and frequency $f = 2.45$ GHz. These results show that the numerical process converged using the default grid. The temperature variations along the centerline of the slot (z = 16 mm) and the catheter surface (r = 0.895 mm) are also presented here in Figures 8a and 8b, respectively. A three-dimensional plot of constant temperature surfaces is given in Figure 9.

(a) Default grid (b) Refined grid

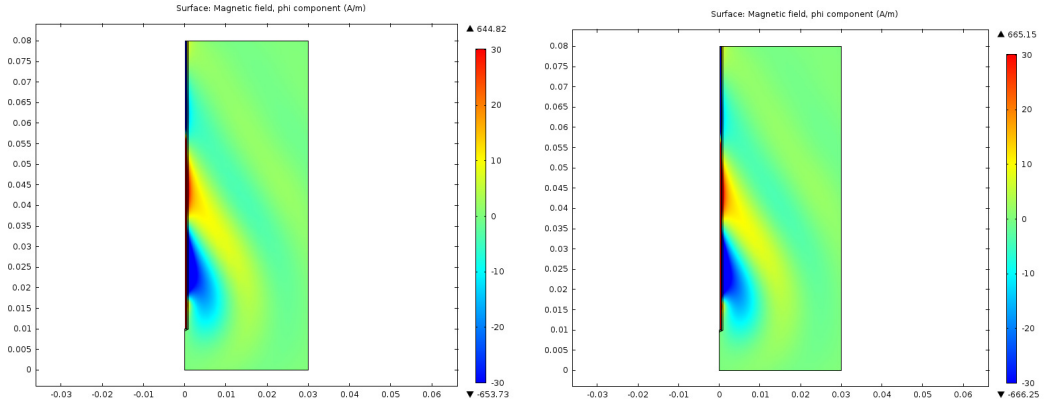

Figure 4. φ component of magnetic field

(a) Default grid (b) Refined grid

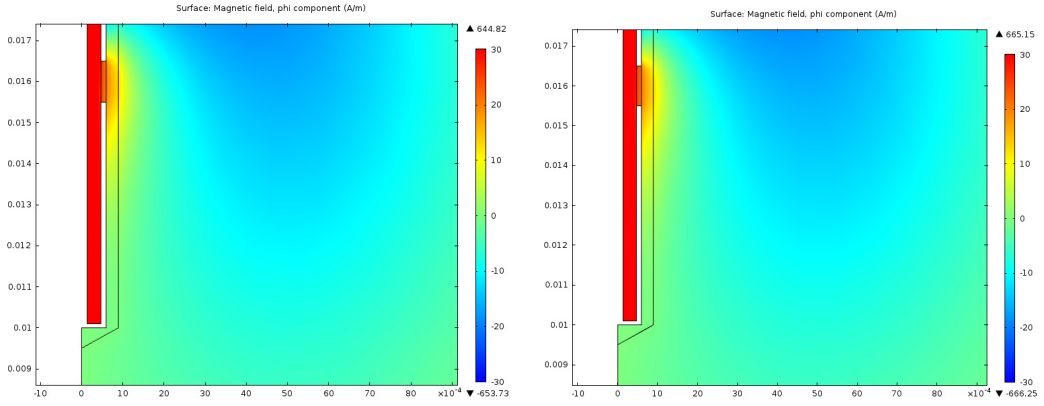

Figure 5. Close-up view of magnetic field near slot

(a) Default grid (b) Refined grid

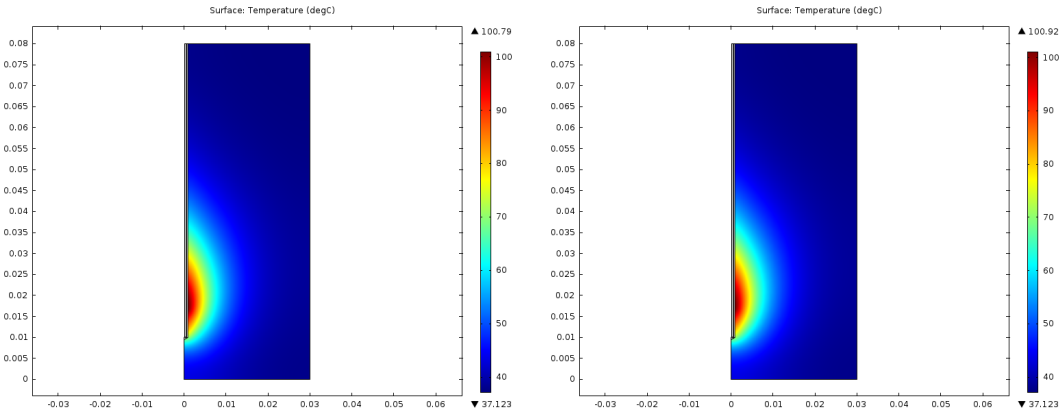

Figure 6. Temperature distribution

(a) Default grid (b) Refined grid

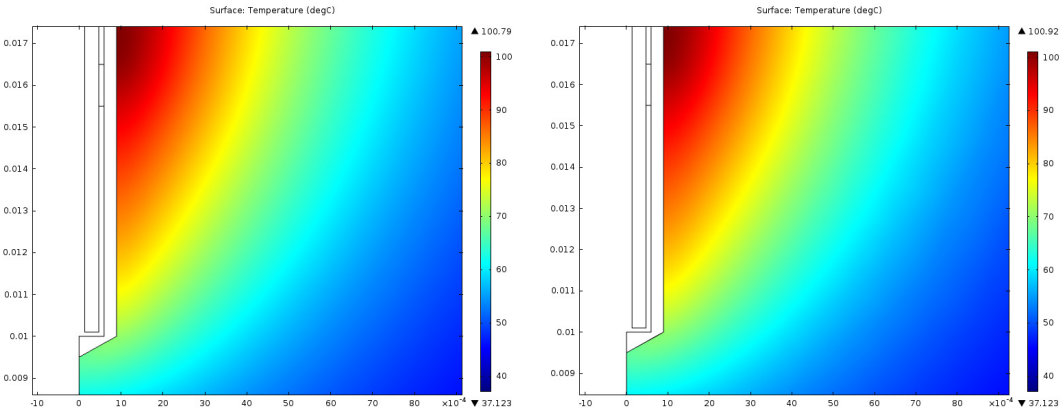

Figure 7. Close-up view of temperature distribution near slot

(a) Center line of slot (b) Catheter surface

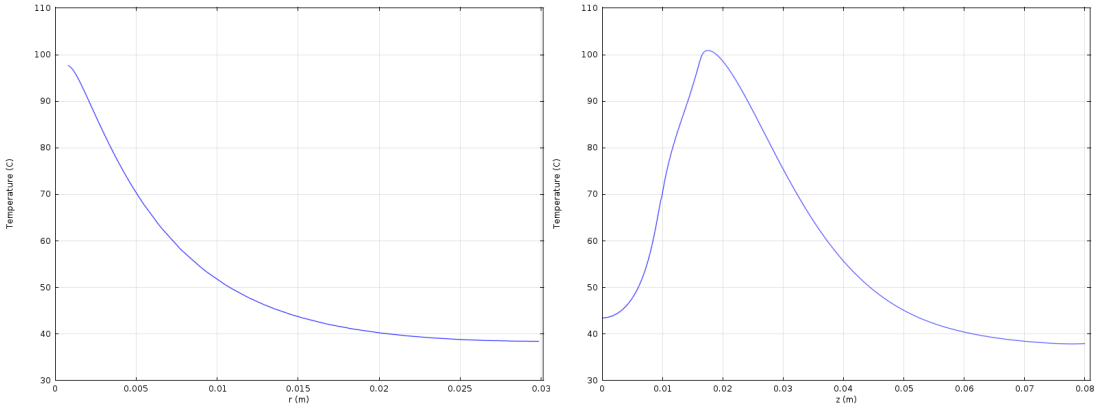

Figure 8. Temperature variation along *r* and *z* axes

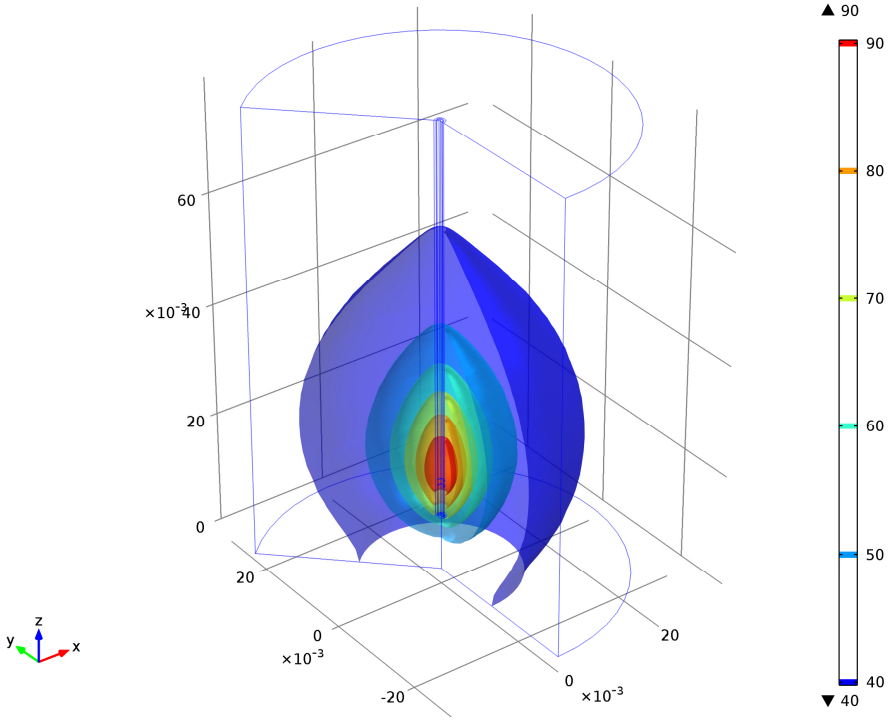

Figure 9. Constant temperature surfaces

The maximum temperature around the antenna is a function of the input power. To find this function, we fixed the frequency at *f =2.45* GHz, which is commonly used in

the therapy. The maximum temperatures are computed for a sequence of power inputs, which are then plotted in Figure 10. Although the temperature is based on the solution of partial differential equations, we find that this relationship is rather simple, in fact, a linear function.

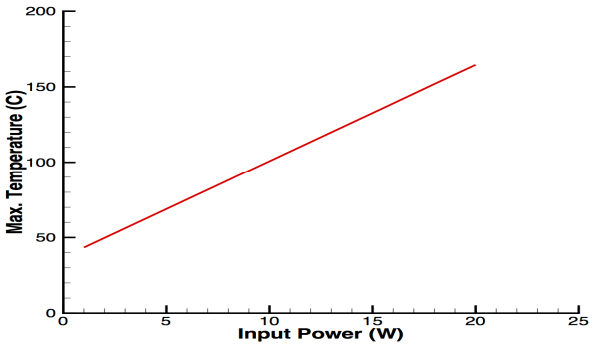

Figure 10. Input power vs. maximum temperature

This linear relationship can also be shown by the mathematical model. Since we assume no heat flux across any boundary surface, Eq. (6) thus gives $Q_{ext} = Q_{pfu}$ on the antenna surface. Using Eqs. (7) and (8), we obtain $T \sim Q_{ext} \sim \left|\vec{E}\right|^2$. From our simulations we find that the maximum temperature always occurs near the slot, approximately 1-2 mm above the centerline, for all levels of input power applied in the numerical experiments. The electric field $\vec{E}$ at the maximum temperature point is therefore closely related to the boundary condition given in Eq. (1). Using Eq. (2), we obtain $\left|\vec{E}\right| \sim \sqrt{P_{avg}}$. Finally, it follows that $T \sim P_{avg}$.

A similar study for the functional relationship between frequency and maximum temperature for a fixed input power, $P = 10$ W, was also carried out. The result is plotted in Figure 11. The green symbols in the figure represent the maximum temperatures at three Industrial, Scientific, and Medical (ISM) Band frequencies, 915 MHz, 2.45 GHz, and 5.80 GHz, respectively. In contrast with the previous case, the maximum temperature exhibits an unsmooth variation at 1.6 GHz, a peak at the most efficient frequency 4.0 GHz, and a sharp decrease around 4.5 GHz. We found that this data can be accurately approximated by a polynomial of degree 9 using a least squares fit, as shown in Figure 12,

$$\begin{aligned}\bar{T} = {} & 0.016 - 0.536f + 7.617f^2 - 61.174f^3 + 304.5109f^4 \\ & - 967.960f^5 + 1947.459f^6 - 2364.381f^7 + 1565.275f^8 - 347.581f^9.\end{aligned} \tag{10}$$

The maximum error of this functional fit is less than 0.5°C.

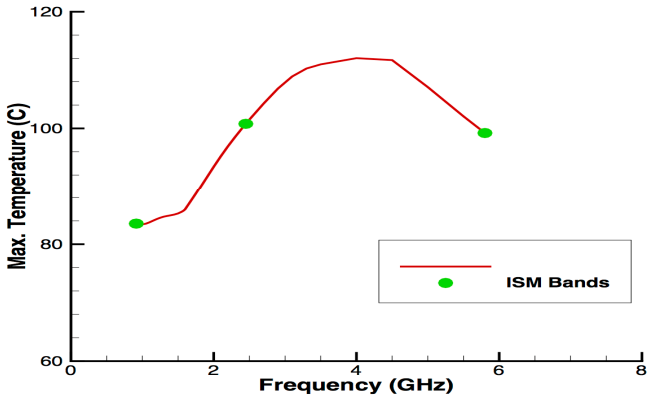

Figure 11. Frequency vs. maximum temperature

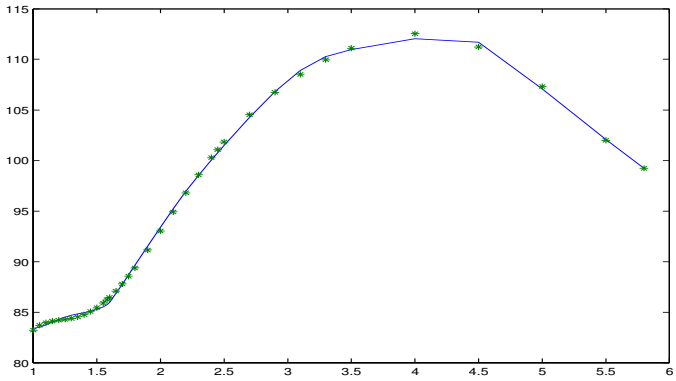

Figure 12. A least squares polynomial fit (stars) for the function of frequency vs. maximum temperature

4. Region of impact

The region in which the temperature is greater than a specified temperature is a critical piece of information for clinical applications. To find a simple model identifying this region, a sequence of simulations were carried out under different power inputs. The region of impact for a given minimum temperature is quantitatively characterized using three values: impact radius, impact area, and impact volume. The contour line positions for the temperature are first interpolated from the solution. One such example is shown in Figure 13 in which temperature contours of 50°C are plotted for different input powers ranging from 3W to 15W at 2W intervals operated at $f = 2.45$ GHz. Corresponding level surfaces are obtained by

rotating the contour lines with respect to the z axis. The impact radius is determined by the maximum value of r from positions of the contour line. The impact area and impact volume are obtained by integrating the area and volume enclosed by the contour line and level surface, respectively. The 50°C impact parameters are shown in Figure 14 for different input powers. Except at low input power for the impact radius, all three impact parameters show an approximately linear relationship with the input power.

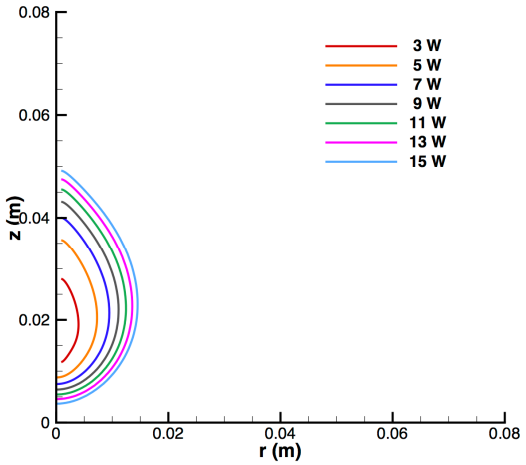

Figure 13. 50°C contour lines

(a) Impact radius

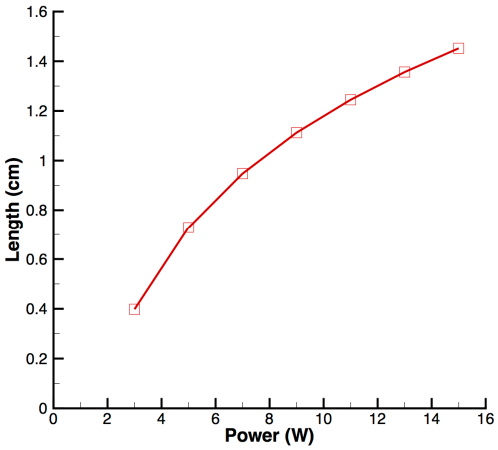

(b) Impact area

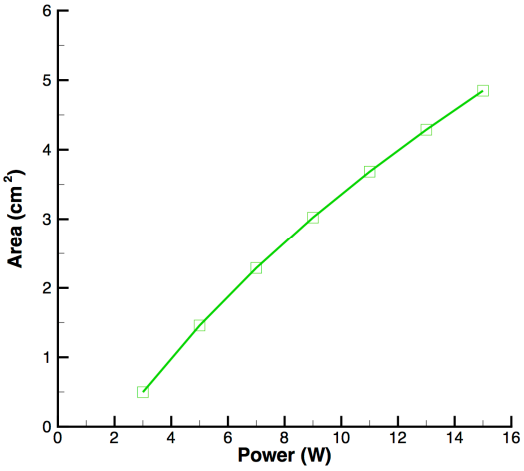

(c) Impact volume

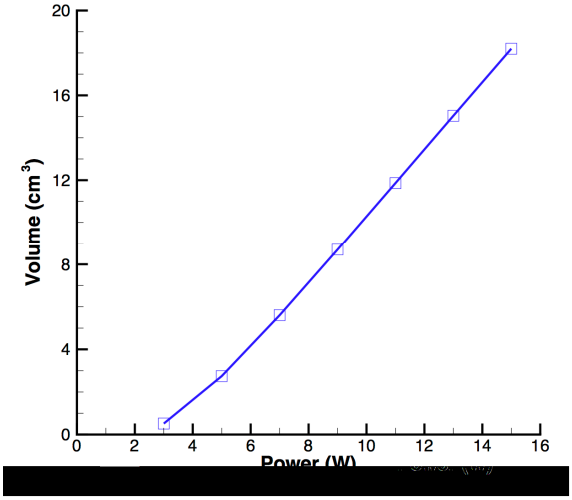

Figure 14. 50°C region of impact

5. Conclusions

We have conducted numerical simulations on microwave coagulation therapy. From the numerical experiments, we conclude that some important relationships in microwave coagulation therapy can be approximately represented by relatively simple functions. This approach of model reduction has the potential benefit of developing simple tools for the improvement of therapeutic effect.

References

[1] P. Prakash, "Theoretical Modeling for Hepatic Microwave Ablation," *The Open Biomedical Engineering Journal*, 4 (2010), 27-38.

[2] R. W. Y. Habash, R. Bansal, D. Krewski, and H. T. Alhafid, "Thermal Therapy, Part 1: An Introduction to Thermal Therapy," *Critical Reviews*^{TM} *in Biomedical Engineering*, 34-6(2006), 459–489.

[3] R. W. Y. Habash, R. Bansal, D. Krewski, and H. T. Alhafid, "Thermal Therapy, Part 2: Hyperthermia Techniques," *Critical Reviews*^{TM} *in Biomedical Engineering*, 34-6(2006), 491–542.

[4] R. W. Y. Habash, R. Bansal, D. Krewski, and H. T. Alhafid, "Thermal Therapy, Part III: Ablation Techniques," *Critical Reviews™ in Biomedical Engineering*, 35(1-2)(2007), 37-121.

[5] R. W. Y. Habash, R. Bansal, D. Krewski, and H. T. Alhafid, "Thermal Therapy, Part IV: Electromagnetic and Thermal Dosimetry," *Critical Reviews™ in Biomedical Engineering*, 35(1-2)(2007), 123-182 (2007).

[6] M. Chaichanyut and S. Tungjitkusolmun, "Thermal conduction and perfusion of ring-slot microwave antenna for treatment liver tumor," International Conference on Biomedical Engineering, Penang, (2012), 450-453.

[7] K. Saito, "Estimation of SAR distribution of a tip-split array applicator for microwave coagulation therapy using the finite element method," Special Issue on Techniques for Constructing Microwave Simulators, IEICE Transactions on Electronics, Vol. E84-C, (2001), 948-954.

[9] COMSOL Multiphysics, version 4.3, 2012, www.comsol.com.

[10] H. H. Pennes, "Analysis of tissue and arterial blood temperatures in the resting human forearm," *J. Appl. Physiol*., vol. 1(1948), pp. 93-122.

Received: July 17, 2013